

IAC-04-IAA.3.8.2.04

THETHERS AS FAR MISSION DESCENT-RETURN TOOLS

Radu D. RUGESCU

PhD. Assoc. Prof. University "Politehnica" of Bucharest, Romania,
Rugescu@yahoo.com

ABSTRACT

Space tethers are investigated as possible future reusable competitive-cost tools for non-gasdynamic descent, landing, takeoff and return from target celestial bodies. The Moon, Mars and a distant planet satellite like Titan are first taken into account as sample mission objectives. The investigation is focused on the mechanical usefulness of the system in comparison with the heavy duty mass expelling energy requirements of equivalent gasdynamic propulsion systems. The two potential categories are (a) the free tether release and return systems and (b) two fixed-points elevator systems. The first one is a further development of the already proposed partial descent system from the Earth ISS adapted to be maneuvered from a robot, remotely flying unmanned spacecraft, up to a complete descent. The second type is an extraterrestrial extension of the proposed Earth based space elevator system and is numerically investigated. Specific deployment techniques prove fitting descent on target bodies with and without an atmosphere. For the case of the Earth, Moon, Europa and similar planetary satellites a free deployment mode is proposed, considering the feasibility of Lunar based, manned deployment maneuvers as solutions of the future. A number of hard technical requirements still remain to be investigated and solutions found, regarding for instance the control of errors in correlation with system dynamics. It proves that, for some of the sample missions analyzed and particularly for the Moon, Europa and Rhea the tethered systems are nevertheless more likely to reach a convenient exploitation stage than the future Earth based space elevator system. This is due to the negligible atmosphere and the low gravity of these moons. It is supposed that the manufacturing technology of light strings will properly mature.

1. INTRODUCTION

Application on space maneuvering for descent and return from far celestial bodies are considered as potential substitutes of the costly rocket propulsion systems, at least in part or temporary. The phase of a free, unpowered deployment and the subsequent orbital evolving of space tethers are under consideration as essential to gain a new thrust in space tethers. A considerable mass of published results are present in the open literature, including those from the two International Conferences on Space Elevators (2001 and 2002), from the five International Conferences on Tethers in Space and at the numerous workshops.

The constant reluctance towards tether systems can only be overcome when significant advantages from the use of space tethers, in this case for distant planetary missions, are proved. The interest lays in the potential for descent and landing to, or return from the surface of the Moon, Europe, Titan or other satellites in the solar system, by avoiding large mass expenses, induced by the conventional rocket propulsion.

There exist already a good practice due to tethered satellites or from suborbital systems (TSS1 and TSS1-R, SEDS-1 and -2, PMG, TiPs and OEDIPUS), but number of questions still persist. Regarding the orbital descent and ascent for example, the question is if tethers offer a better alternative to rocket propulsion.

It is required to demonstrate that the deployment of large strings from orbiting vehicles is reliably achievable and this can be performed without any assistance from propulsion systems, meaning no mass consumption and thus much cheaper. And that these systems are accurately controllable. Numerical simulation was the basic tool in the present approach.

The deployment technique here adopted is called "free tether", as far as friction-like or other kinematical restrictions on the deploying string are neglected. The deployment is essentially based on implementing a given, small velocity impulse between the main orbital object and the tethered mass, or between equal tethered masses with a relative velocity impulse below 15 m/s, achieved by small size spring or pyrotechnical means. The masses are thus inserted into different orbits that end in a continuous departure between each-other, up to a convenient distance that will be eventually set constant at *connection*².

It is known that a continuous departure of the objects only occurs in the condition of a horizontal initial impulse, while a vertical separation induces repeated rejoining at each complete orbit. Numerical simulations show that the horizontal expel is a feasible one, as far as any gasdynamic control is avoided.

The next milestone is the stop of deployment, or connection, at the desired tether length. The problem of connection is essentially a matter of mechanical collision avoidance, or the radial relative velocity suppression at the connection moment. While moving free in orbit, favorable circumstances occur after the end of each orbit from the deployment start (DS) where a collision-free connection is possible. When these favorable positions are not followed, shock-type discontinuities in the motion of the tethered system intervene, absorbed in part by the elasticity of the system but tending to end in a global tether system instability. Computations also show that a residual momentum always persists after connection and inevitably sends the system into a "dumbbell libration" (Lorenzini³).

2. NON-GASDYNAMIC DEPLOYMENT

The following assumptions are considered consistent with the case of study:

- the gravity field is spherical, without non-symmetrical components;
- astronomical perturbations of the Moon and Sun are negligible;
- the orbiting masses are material points associated to their center of mass, without any transverse dimensions;
- the mass and weight of the tether string are negligible;
- the material of the tether is a h-p-c. flexible while inelastic;
- no time relaxation occurs.

A detailed evaluation of this assumption was performed elsewhere¹ and shown that they serve the cause of the study. Consequently, the elliptical motion only of the splitting masses is considered here, after their horizontal impulse separation (HIS). Prior to HIS, a circular satellite orbit is assumed for the undeployed tether, with the connected objects moving at the constant altitude h_0 with the circular absolute velocity $w_0 = \sqrt{K_{\oplus}/r_0}$, where K_{\oplus} is the gravity constant of the Earth.

At the DS moment ($t = 0$) the velocity impulse Δw_0 is administered in the direction of flight and, denoting by $\mu = m/M$ the ratio of masses of the accelerated and decelerated objects respectively, the two bodies enter separate orbits with the insertion velocities

$$v_0 = w_0 + \frac{1}{1 + \mu} \Delta w_0, \quad V_0 = w_0 - \frac{\mu}{1 + \mu} \Delta w_0.$$

The corresponding orbits (polar coordinates) of the accelerated and lower-orbiting masses respectively, behaving with eccentricities ε and E , are described by:

$$r = \frac{p}{1 + \varepsilon \cos(\theta - \theta_0)}, \quad R = \frac{P}{1 + E \cos(\Theta - \Theta_0)}.$$

In the given circumstances the insertion point for the upper mass is located in its apoapsis and for the lower one in its periapsis.

Assuming the common space-time origin at these specific points (θ_0 and $\Theta_0 = 0$, namely $r_P = R_A = r_0$) and using the Vis-Viva energy equation also, the two orbits are described by

$$r = \frac{P}{1 + \varepsilon \cos \theta}, \quad v^2 = K_{\oplus} \left(\frac{2}{r} - \frac{1}{a} \right),$$

$$R = \frac{P}{1 - E \cos \Theta}, \quad V^2 = K_{\oplus} \left(\frac{2}{R} - \frac{1}{A} \right). \quad (1)$$

During the successive orbits the velocity of the upper object develops low and the speed of the lower object performs high than at HIS

Based on the conditions at insertion the orbital parameters derive

$$\varepsilon = r_0 \frac{v_0^2}{K_{\oplus}} - 1, \quad a = \frac{r_0}{1 - \varepsilon}, \quad p = r_0(1 + \varepsilon)$$

$$E = 1 + r_0 \frac{V_0^2}{K_{\oplus}}, \quad A = \frac{r_0}{1 + E}, \quad P = r_0(1 - E)$$

A continuous drift between the two independent bodies begins, the faster mass M from beneath running always in front of the slower mass m in respect to the soil. The relative distance d gradually increases and this motion is the basis of the *free tether deployment*.

A simple analytical description results where a special care is only required to the time synchronization procedure, with reset of time origin for the upper body after each complete orbit of the inner mass. A common time reference is most recommended. Appeal is now made to the Kepler first integral to provide the local time:

$$t = \frac{T_m}{2\pi} (\nu - \varepsilon \sin \nu), \quad T_m = \frac{a}{v_0} \sqrt{\frac{1 + \varepsilon}{1 - \varepsilon}},$$

$$t = \frac{T_M}{2\pi} (N + E \sin N), \quad T_M = \frac{A}{V_0} \sqrt{\frac{1 + E}{1 - E}}. \quad (2)$$

In relations (2) the corresponding eccentric anomaly of the upper mass m is denoted by ν and for the lower mass M by N , while the corresponding periodic times of orbital motions are T_m and T_M respectively.

Time is measured from the common space origin, where the HIS occurred, that means from the periapsis of mass m and from apoapsis of mass M .

Expressed directly from the input data of insertion, these periodic times are given by

$$T_m = \frac{2\pi a^2 \sqrt{1 - \varepsilon^2}}{r_0 v_0}, \quad T_M = \frac{2\pi A^2 \sqrt{1 - E^2}}{r_0 v_0}.$$

The computational sequence for this twin-constellation flight is thus

$$Data \rightarrow t(\text{common}) \rightarrow v_1, v_2 \rightarrow \theta_1, \theta_2 \rightarrow \{x_1, y_1, x_2, y_2\}.$$

The Gauss substitution² transfers the eccentric anomalies into the true anomalies:

$$\operatorname{tg} \frac{\nu}{2} = \sqrt{\frac{1 - \varepsilon}{1 + \varepsilon}} \operatorname{tg} \frac{\theta}{2}, \quad \operatorname{tg} \frac{N}{2} = \sqrt{\frac{1 - E}{1 + E}} \operatorname{tg} \frac{\Theta}{2}. \quad (3)$$

These are the space references for eccentric and true anomalies and must lay in the eigen-periapsis of each orbit. It is a convenient transform that establishes correlation with the formulae (1).

3. COMPUTATION OF DEPLOYMENT

Although the formulated constellation flight problem does not require numerical integration of ODE-s and the solutions are direct, special precautions are mandatory in order to receive correct results. The continuous surveillance of position on each orbit and correct positioning of time origin is one. The Kepler equations (2) require a Newton-Raphson iterating solution to render the eccentric anomaly at a simultaneous time value. Due to the fact that the relative motion of the constellation bodies has extremely diverse amplitudes, while the Earth-body distance remains always high, the numerical code can only be run in double precision.

The motion is referenced to a frame bound to the orbiting point where the two bodies were stuck together prior to HIS. Although virtual, this point is the best reference to observe small nonlinear effects during separation and deployment of the tether system.

Bear in mind that this is the place which the bodies would have been moving further with if the separation had not occurred.

In the nearby Fig.1 several deployment local trajectories are drawn for an LEO system at $h_0 = 160$ km, equal masses $\mu = 1$ and $\Delta w_0 = 1, 2, 3, 4$ and 5 m/s. They are specifically aligned under the same height angle as seen up from the starting point O when the connection occurs after the same time interval. In the case of Fig. 1 the common duration of deployment is 2100 seconds and the common height angle is 34.9° , no matter how great the separation impulse Δw_0 is.

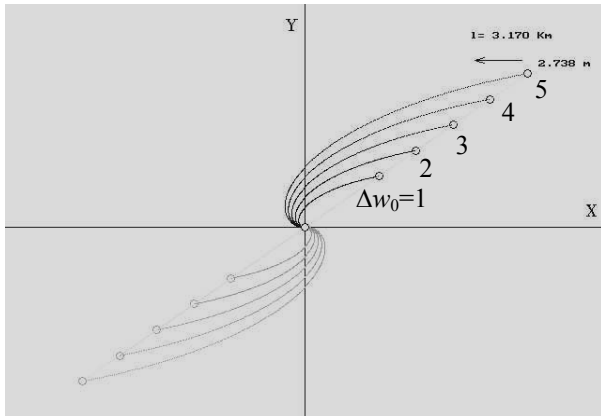


Fig.1: Free tether deployment for 2100 s.

The angular amplitude of the motion does not depend on the initial relative velocity, as consequence of conservation of moment of momentum and because the local referential moves almost rectilinear on a short scale.

At such a local scale the motion of the twin masses in respect to the starting pole O preserves almost entirely symmetrical. At larger scales this symmetry gradually vanishes, due to planet curvature. The entire motion remains planar, due to the fact that the separation impulse was definitely directed into the plane of the orbital motion. This case proves to be the one of practical use.

An orbit-long deployment phase is required to attain a zero radial velocity \dot{d} at connection. An example of such a deployment procedure for $\Delta w_0 = 1, 2$ and 3 m/s is given in Fig. 2 as it results from running the *FREETETH* code.

Some 5850 seconds of deployment are required, ending in a radial velocity along the tether of below 7 mm/s. The transverse velocities of the end-masses remain however important and eventually induce a global rotation of the tether system after connection.

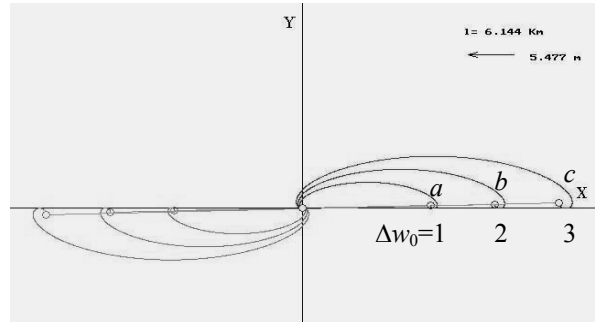


Fig.2: Free tether deployment to 5850 s.

The velocity magnitude transmitted at tether connection is analyzed in the next chapter. For the moment nothing can prove however that the eventual motion of the system remains stable. This aspect is answered in the following chapters. The relative motion of departing masses continues in chained loops after each complete orbit.

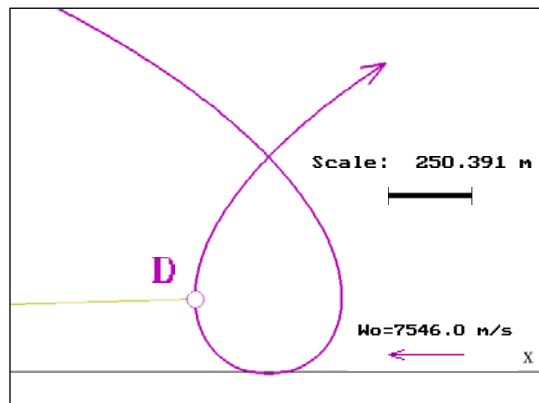


Fig.3: Best tether connection point D .
(Zoom at end of loop a in Fig.2)

The relative trajectory of the upper mass m along the turning loop on the end of its first orbit and the initiation of the second one, for the same $\mu = 1$ and $h_0 = 160$ km above the Earth is given in Fig.3, with the point of the smooth connection ($\dot{d} = 0$) marked as D . On its relative motion the mass goes from upper left to upper right (arrow).

The straight line near the bottom in the draft is the X-axis, with the origin in the orbiting initial point of the undeployed system, some 7 km to the left. The short, left oriented line emerging from the best connection point D is the tether itself, pointing towards lower mass of the tether system at left, not visible in the image. The draft scale is of 1800 meters in horizontal width of the frame as marked.

Whenever longer tethers are devised, the smooth connection must wait until a convenient number of orbits are passed. While zero longitudinal relative velocity along the string is attained, the tethered system preserves a transverse rotation into its orbital plane, less and less energetic with each elapsed orbit.

The eventual motion of the tethered system depends on the peculiar conditions fulfilled at connection. The components of the speeds are given by

$$\mathbf{v} = \dot{r}\mathbf{p} + r\dot{\theta}\boldsymbol{\tau}, \quad \mathbf{V} = \dot{R}\mathbf{R} + R\dot{\Theta}\mathbf{T},$$

$$\dot{d} = (r\dot{r} + R\dot{R} - (rR + r\dot{R})\cos\delta + rR\dot{\delta}\sin\delta) / d \quad (4)$$

These are the entering values for the connection process of the orbital system.

4. TETHER CONNECTION

At the *connection point* (CP), meaning at the very moment when the planned tether length is attained and the tether deployment is instantly blocked, during that short time interval the conservation laws of momentum and moment of momentum show that these parameters keep constant as far as internal forces are only present. Negligible small variations in the external forces occur and consequently one may write:

$$\mathbf{H}_c - \mathbf{H}_e = \int \mathbf{F} dt \approx \mathbf{F} \Delta t, \quad \Delta t \rightarrow 0, \quad \mathbf{H}_c = \mathbf{H}_e, \quad (5)$$

$$\mathbf{K}_c - \mathbf{K}_e = \int (\mathbf{r} \wedge \mathbf{f} + \mathbf{R} \wedge \mathbf{F}) dt \approx \mathbf{M}_F \Delta t,$$

$$\Delta t \rightarrow 0, \quad \mathbf{K}_c = \mathbf{K}_e. \quad (6)$$

While the kinetic moment, moment of momentum and the position of the masses are insignificantly altering, the speed components manifest drastic changes.

The following relations (see also Fig.4) account for the conservation laws:

$$\begin{aligned} \dot{r}_c &= \frac{K_{Me}}{ml} \sin\psi + \frac{H_{le}}{1+\mu} \cos\psi, \\ r\dot{\theta}_c &= \frac{H_{le}}{1+\mu} \sin\psi - \frac{K_{Me}}{ml} \cos\psi, \\ \dot{R}_c &= \frac{K_{me}}{Ml} \sin\Psi - \frac{H_{le}}{1+\mu} \cos\Psi, \\ R\dot{\Theta}_c &= -\frac{H_{le}}{1+\mu} \sin\Psi - \frac{K_{me}}{Ml} \cos\Psi, \end{aligned} \quad (7)$$

where

$$\begin{aligned} H_{le} &= \mu(\dot{r}_e \cos\psi + r\dot{\theta}_e \sin\psi) - \dot{R}_e \cos\Psi - R\dot{\Theta}_e \sin\Psi, \\ \frac{K_{me}}{Ml} &= \dot{R}_e \sin\Psi - R\dot{\Theta}_e \cos\Psi, \\ \frac{K_{Me}}{ml} &= \dot{r}_e \sin\psi - r\dot{\theta}_e \cos\psi. \end{aligned} \quad (8)$$

The symbols used and the geometry of the tethered orbiters are shown in Fig. 4.

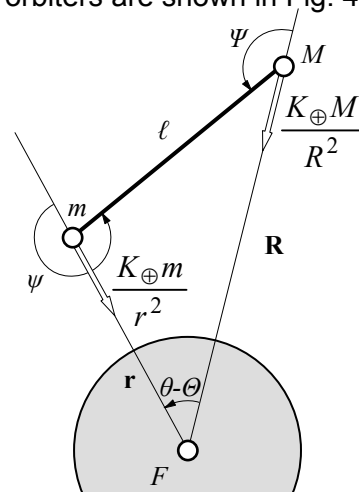


Fig.4: Tether geometry under gravity.

The set (7) of kinematical conditions assure the transfer from the preliminary free motion of the tether end-masses to the definite motion of the connected system after stop of deployment. They determine the tether motion as eventually subjected to an important gravity gradient. No closed, analytical solutions for this motion are available^{2,4,6}. Numerical computation of the actual tether orbital evolution was further performed by convenient simulation codes that are presented below.

5. INTEGRATION OF TETHER EQUATIONS

The problem of the description of tether orbital motion is considerably complicated by some intrinsic numerical difficulties of the problem. This are mainly related to the following areas:

- large discrepancies at the scale level between the local distances and the astro-centric distances;
- very small astro-centric angular contrast between the tethered masses;
- extremely large discrepancies between the relative velocities of the masses and the orbital absolute velocity of the whole system.

The last peculiarity is highly aggravated at those positions where the tether goes horizontally in respect to the local surface of the planet. All these features impose a careful treatment of the numerical solution. The manner in which the very variables of the astro-mechanical description are chosen proves to have a deciding role for the convergence of the computational scheme.

To enhance the accuracy the variables involved in successive computations were first declared as *double precision*. A fourth-order Runge-Kutta numerical integration method was then adopted as properly accurate. Analyze of the mathematical formulation shows now that the 2-D problem is governed by 3 degrees of freedom and consequently require adoption of a set of 3 dependent variables. Two options were successively considered regarding the kinematical restriction $\ell = const.$

5.1. Scheme A: double-differential restriction

To remain close to the treatment of the free deployment motion the set of variables was chosen as $\{\theta, \Theta, r, R\}$ at a preliminary stage.

The fourth variable was introduced to account for the restriction $\ell = const.$ as an extra ODE, resulting from the double differentiation of $\ell = const.$ condition. Thus one equation in $\ddot{R} = 0$ derives from the double-differential restriction $\ddot{\ell} = 0$ and is added to the system.

Consequently, the four resolving equations are written in the following working form (9) as a system of second order ODE-s:

$$\left\{ \begin{array}{l} Q \equiv \left[\frac{K_{\oplus}}{\ell} \left(\frac{\cos \psi}{r^2} + \frac{\cos \Psi}{R^2} \right) + \omega^2 \right], \\ \ddot{\theta} = -2 \frac{wu}{r} - \frac{R \sin(\theta - \Theta)}{(1 + \mu)r} \cdot Q, \\ \ddot{\Theta} = -2 \frac{ZV}{R} + \frac{\mu r \sin(\theta - \Theta)}{(1 + \mu)R} \cdot Q, \\ \ddot{r} = ru^2 + \frac{R \cos(\theta - \Theta) - r}{1 + \mu} \cdot Q - \frac{K_{\oplus}}{r^2}, \\ \ddot{R} = RV^2 - \mu \frac{R - r \cos(\theta - \Theta)}{1 + \mu} \cdot Q - \frac{K_{\oplus}}{R^2}. \end{array} \right. \quad (9)$$

In this transcription the following geometric and kinematical relations are used (with the keys given in Fig.4):

$$\left\{ \begin{array}{l} \ell \cos \psi = R \cos(\theta - \Theta) - r, \\ \ell \cos \Psi = r \cos(\theta - \Theta) - R, \\ \ell \sin \psi = -R \sin(\theta - \Theta), \\ \ell \sin \Psi = r \sin(\theta - \Theta), \\ \ell \omega^2 = (R \ddot{\Theta} + 2 \dot{R} \dot{\Theta}) \sin \Psi + (\ddot{R} - R \dot{\Theta}^2) \cos \Psi + \\ + (r \ddot{\theta} + 2 \dot{r} \dot{\theta}) \sin \psi + (\ddot{r} - r \dot{\theta}^2) \cos \psi. \end{array} \right. \quad (10)$$

In the Kane form, ready for numerical integration, the equations read

$$\left\{ \begin{array}{l} \dot{\theta} = f_{\theta}(u) \equiv u, \\ \dot{u} = f_u(\theta, \Theta, r, R, u, w), \\ \dot{\Theta} = f_{\Theta}(V) \equiv V, \\ \dot{V} = f_V(\theta, \Theta, r, R, V, Z), \\ \dot{r} = f_r(w) \equiv w, \\ \dot{w} = f_w(\theta, \Theta, r, R, u), \\ \dot{R} = f_R(Z) \equiv Z, \\ \dot{Z} = f_Z(\theta, \Theta, r, R, V). \end{array} \right. \quad (11)$$

Although apparently feasible, for *prolonged time periods* this integration scheme proved basically non-consistent and the equation $\ddot{\ell} = 0$ unusable. Hence the geometrical restriction $\ell = const.$ should be accounted in a much direct manner.

5.2. Scheme B: direct geometric restriction

When one of the above used dependent variables, responsible for the non-consistency is removed, say \mathbf{R} in this case, the geometric restriction regarding the length of the tether is directly used to find that value of \mathbf{R} and the number of computational ODE-s is reduced to three. While the set of directly dependent variables now consists of $\{\theta, \Theta, r\}$, for the radius vector \mathbf{R} , namely for its magnitude R and its variation \dot{R} the relations are used:

$$\begin{cases} \delta = \theta - \Theta, \\ \ell \cos \psi = R \cos \delta - r, \\ \ell \cos \Psi = r \cos \delta - R, \\ \ell \sin \psi = -R \sin \delta, \\ \ell \sin \Psi = r \sin \delta, \\ R = r \cos \delta \pm \sqrt{\ell^2 - r^2 \sin^2 \delta}. \end{cases} \quad (12)$$

One inevitable uncertainty is introduced by the undetermined sign in the last formula for R , physically induced by the existence of two possible solutions of the geometrical problem. This is solved by checking the continuity of variation of value R and counting the sign of its derivative. This is an example only of the multiple numerical challenges of the scheme which are to be solved when a solid algorithm is to be built.

The value of \dot{R} is further extracted from the condition $\dot{\ell} = 0$ that reads

$$\dot{R} = -\frac{\dot{r} \cos \psi + r \dot{\theta} \sin \psi + R \dot{\Theta} \sin \Psi}{\cos \Psi}. \quad (13)$$

At almost all the situations encountered the above algorithm proves consistent. It was observed however that at horizontal positions of the tether, namely where \dot{R} approaches zero, anticipation of the solution (12) for R becomes uncertain. At these particular circumstances a temporary return to the scheme involving the forth equation in \ddot{R} proved useful and reliable. To avoid sensible distortions this local smoothing is applied for a very limited number of computational steps.

One notes however that this escape procedure, although proved as highly efficient

so far, has an insufficiently proved foundation and needs further investigation. Worth saying that similar numerical description of tether motion was not yet found elsewhere in the open literature.

6. NUMERICAL RESULTS

Once the solver of the boundary conditions problem developed, a lot of simulations were performed with different initial conditions for the connection of the tether, both in Earth and Moon orbits.

These simulations revealed important peculiarities of the tether motion while orbiting a low Earth orbit of 100 miles altitude and confirmed some of the observed features⁴. The LEO motion was first considered that starts when the tether extension ends at the best connection point (where $\dot{\ell} = 0$), after one orbit of deployment, involving 1 m/s initial velocity. The phase of preliminary deployment is that represented in Fig.2-a. The spherical Earth constants used all along are $K_{\oplus} = 3.987624457 \cdot 10^{14} \text{ m}^3/\text{s}^2$ for the gravity parameter and $r_{\oplus} = 6371221 \text{ m}$ for the mean Earth radius.

Long after connection, the trajectory followed by the tether is drawn in Fig.5 and 6, where the schemes A and B were successively used for comparison. The false trajectory delivered by the scheme A with 4 ODE-s (Fig.5) supports the previous statement that this procedure cannot preserve correctly the constant length of the tether after connection.

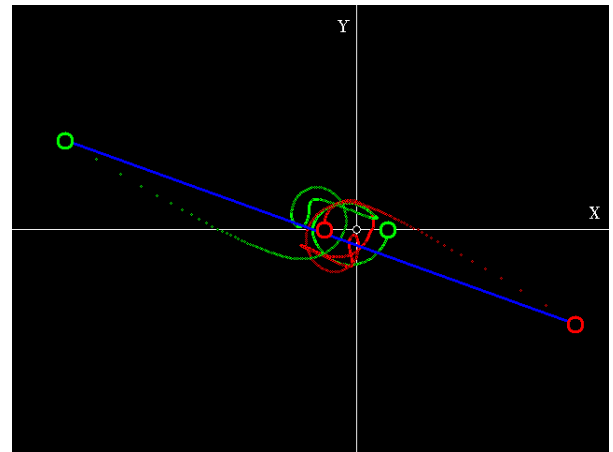


Fig.5: Sample of false trajectory by scheme A.

The scheme B on the contrary, limited on substitutions for the values of R and \dot{R} only, is strongly reliable for long term. The draft in Fig.6 is limited to three orbits only, but computations went flawlessly up to over a hundred orbits. It is an exercise in support of the computational method only, because the tether itself behaves unstable.

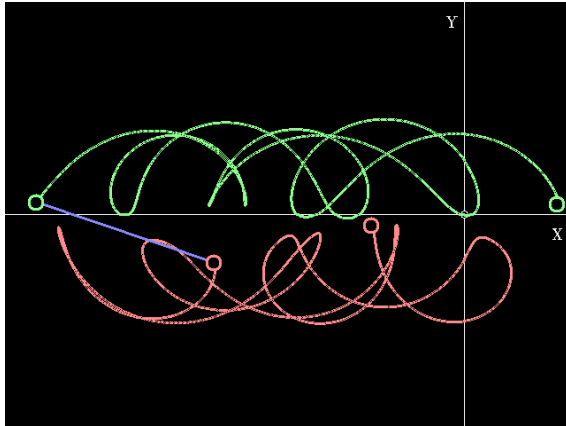


Fig. 6: True Tether trajectory by scheme B.

When the deployment phase ends in advance of the smooth connection point, the tether enters a libration motion which eventually preserves stable (Fig. 7). The oscillations manifest amplitudes of about 50 degrees that do not depend on where the connection was performed. This is valid however when CP is located prior to a margin of 80% of the total orbital loop. After that limit the tether will enter a wobbled rotation that becomes unstable.

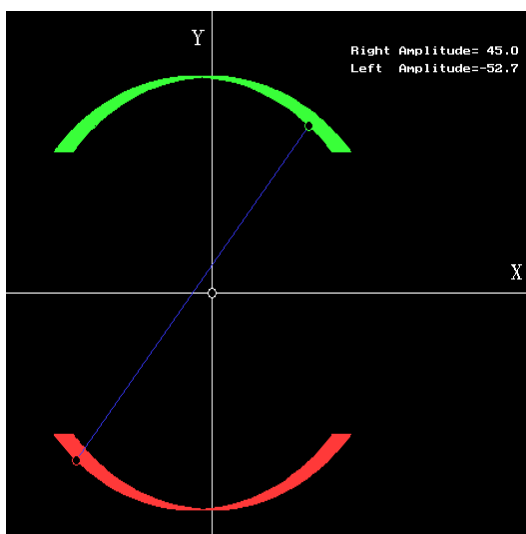


Fig.7. Libration motion after a vertical connection.

The libration remains stable for very long periods if associated to the local vertical of the tether mass center. In the given example, after five orbits the libration amplitude remains equal to the one at the beginning of flight, with the value of 49° , close to orbital observations on existing tether satellites. The constant amplitude gainsays some data^{2,4}.

6.1. Mass center motion in LEO

The trajectories of the center of mass themselves are always blurred in a curly-type waving motion that suggests a sort of hysteretic energy dissipation process (Fig. 8). In the given example the tether is deployed smoothly at the end of the first orbit and a length of 58.056 km is engaged. The summing effect is a continuous drift of the mass center in the direction of flight. The velocity of this drift depends on the initial "sink" of the system, inherited at the CP and provided by the planet curvature. Along with that drift a continuous change in the curl amplitude manifests, resulting in a gradual change in the tether oscillations.

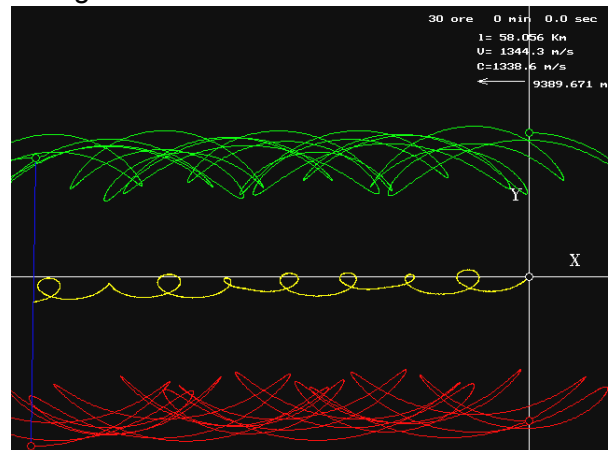


Fig. 8: Center of mass during libration.

After ten orbits or 26 hours and 7 minutes at the altitude of 160 km a drift of more than 150 km accumulates and the vertical amplitude of CM oscillations equals some 6 km. The computed motion looks quasi-periodic, but it hardly suggests possible analytical solutions for the tether motion.

The observed damping of librations on existing satellites is possibly due to the high atmosphere drag, very small and not accounted in the present computations.

6.2. Free tether in lunar orbit

Computations used $K = 4.9047848 \cdot 10^{12} \text{ m}^3/\text{s}^2$ and $r_l = 1737400 \text{ m}$ for the lunar gravitational parameter and its radius. The lunar behavior looks similar to the terrestrial one^{8,9,10}, with a slower motion however (Fig. 9).

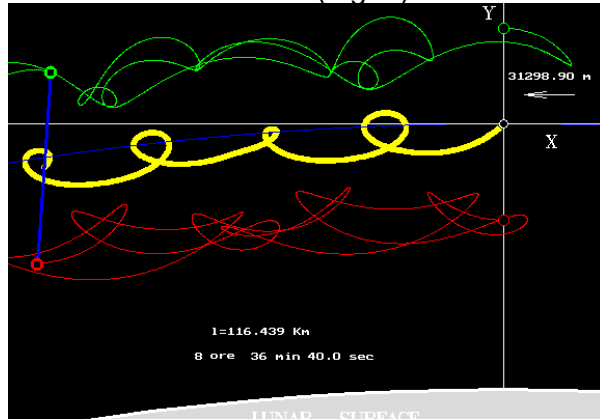


Fig. 9: Libration in low lunar orbit.

On a 1000 km altitude Moon orbit (circular velocity 1338.6 m/s), equal masses with a HIS of 80.5 m/s and a 4590 seconds deployment produce a tether length of 800 km and typical librating motion with a long periodic time. The center of mass (MC) moves on a large sinking trajectory (200 km under the reference orbit) that exhibits the shape of a perfect gravity coupled hexagon (Fig. 10, yellow line for MC). The 360 degrees drift is completed in 23 hours and 19 minutes after exactly six lunar orbits. Amazing is that, despite the apparent irregularity of the tether trajectory, the hexagonal cycle is repeating with hard persistence. It is also surprising to observe a complete symmetry of the motion about an axis (white-dashed line in Fig. 10) positioned at 30° in front of HIS orbiting point. This repeatability makes a proof also for the numerical solution, which could not have multiplied so exactly in the presence of computational errors.

The lower mass is approaching the lunar soil to less than 5 kilometers on the high velocity branch (1433.3 - 1678.3 m/s at LP). On the reverse branches, the local velocity lowers with a good 500 m/s, not low enough to attempt landing. These results suggest however that altitude-HIS combinations exist where lunar landing becomes accessible.

Possible configurations for convenient lunar landing require very long tether deployment.

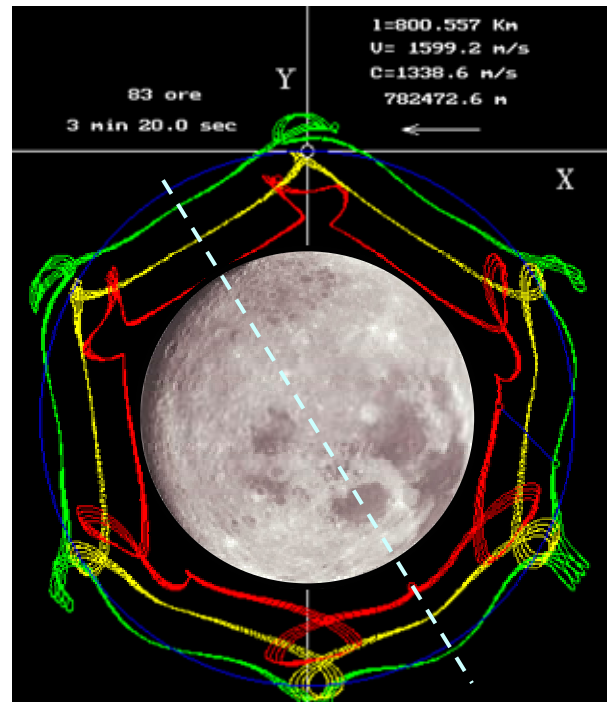


Fig. 10: Lunar perfect gravity coupling.

6.4. Lunar landing with tether

High lunar orbits were further investigated on tethers with unequal masses in long free deployment. Unequal masses diminish the vertical oscillations and the forward and backward branches become equally frequent. The low relative velocities to the soil can be easily exploited. Provided the technological problems related to ultra long tethers are solved, configurations appeared where a safe lunar landing is feasible (Fig. 11).



Fig. 11: Soft lunar landing with tether.

The mass ratio of 1:16 at initial orbit of 935 km altitude ($w_0=1354.8$ m/s) and three orbits deployment with a HIS of 8.7 m/s produces a tether length of 939.7 km. It is exactly the amount required to position the smaller end mass at 500 m above the lunar soil with the negligible 10 cm/s relative velocity! The soft landing with 10 m/s velocity expense in orbit only is proved. Incidents in case of mistargeting seem largely diminished due to negligible relative velocity around LP.

6.5. Tethers for Europa and Rhea missions

Numerical simulations were also performed to investigate conditions for a safe landing on Jupiter’s moon Europa and for Saturn’s Rhea, down from parking orbits around this moons. Values of $K_E = 3.20419804 \cdot 10^{12}$ m³/s² and $r_E = 1561000$ m were considered for Europa, respectively $K_R = 1.542020305 \cdot 10^{11}$ m³/s² and $r_R = 764000$ m for satellite Rhea^{10,11}. Again a gravity resonance manifests in the European orbit. Decagonal geometry is given in Fig. 12 for an orbit at 1000 km above Europa and a tether deployment for 6000 seconds to 750 km, after HIS maneuver of 34.75 m/s.

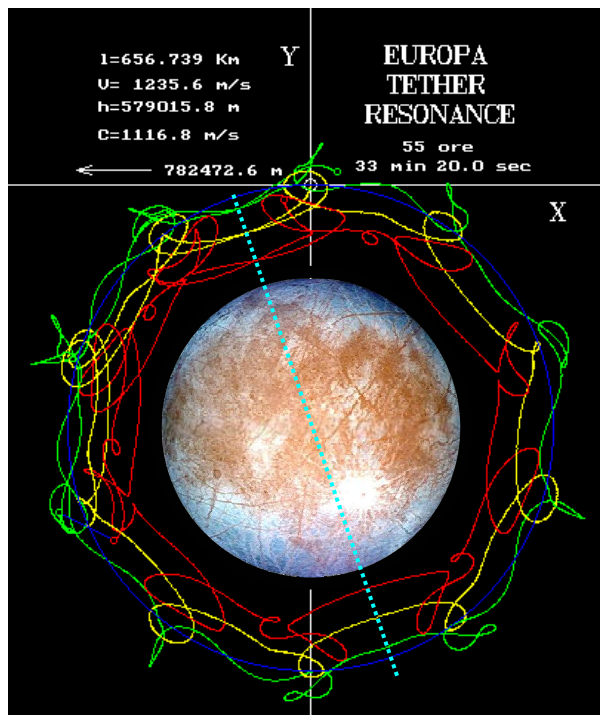


Fig. 12: European tether decagonal resonance.

A 19° symmetry line for the resonant orbit (blue dashed line) is present again.

Soft Europa tethered landing from an orbit at 810.5 km after 7.27 m/s HIS and optimal third orbit connection, with a tether length of 816 km is given if Fig. 13. The tether must annihilate the circular velocity of 1160.4 m/s for landing. The 1/30 payload-orbiter mass ratio produces an approach to 178 m altitude with 10 cm/s residual velocity.

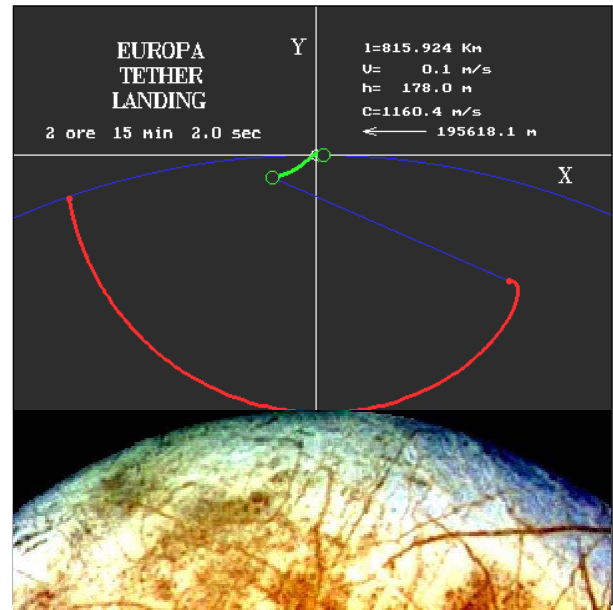


Fig. 13: Landing on Europa.

For the flight about Rhea a beautiful pentagonal configuration of resonance is drawn in Fig. 14 from numerical simulations.

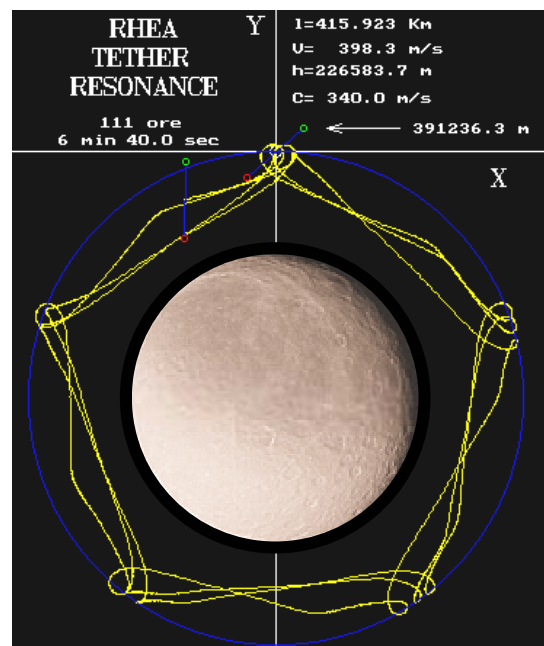


Fig. 14: Rhean pentagonal resonance.

A two-fold orbital replication seems to characterize the flight condition for the Rhean tether.

7. CONCLUSIONS

The accurate numerical simulation of both equal and non-equal, twin-mass tether systems in LEO and around other bodies shows possible unpowered deployment scenarios with consequent stable librating motion of the system, when the connection between the two end-masses is settled in advance of the smooth point of connection. For time intervals below one sidereal day little if any extinguish process was found on the oscillatory motion. The entire study was performed under convenient, simplifying assumptions.

The stability of the tethered masses was accounted by calculating the variation of the force in the string. A stable configuration means a positive value of the tension. The librating motion proves always stable, while the tumbling rotation ends always in instability. This is a challenge for tether

landing, as repeated approach of the lunar soil is highly desirable for a safe landing.

Combinations of HIS velocities and altitudes are always found which provide a convenient soft landing, but this greatly depends on the initial conditions of flight and deployment. A high precision of maneuvers is required to assure the success of the landing.

The found configurations are once-in-a-try type, fact that presents a major challenge. Tether evolution in case of an abandoned landing is however less attractive because the string enters unstable behavior short after the transit through LP. The tether position drawn in Fig. 11 and 13 corresponds to the end of stability phase (magenta indicator for the tether). It means that the landing tentative can not be repeated in case of a first failure and this represents a very adverse condition. This is why three-mass tethered systems are conceived, but equal deployment of very long three-mass tethers is questionable.

Bucharest, on August 24, 2004.

REFERENCES

1. B. C. Edwards, *The Space Elevator in Science Fiction and Reality*, paper IAA.8.2.08, session Innovative Space Technologies-in Science Fiction, 54th International Astronautical Congress, Bremen, Germany, 01 October 2003;
2. E. Messerschmid, S. Fasoulas, *Raumfahrtsysteme, Chap.4.6 Tethers im Gravitationsfeld*, Springer, Berlin, Heidelberg, 2000;
3. E. C. Lorenzini, *Novel Tether-Connected Two-Dimensional Structures for Low Earth Orbits*, Journal of the Astronautical Sciences, Vol. 36, No. 4, p. 389-405, Oct.-Dec. 1988.;
4. M.L. Cosmo and E.C. Lorenzini, *Tethers in Space Handbook*, NASA Marshall S.F.C. Grant NAG8-1160, 1997;
5. Steven E. Patamia, *Space Elevator Transverse Oscillations with Free Boundary Conditions*, The Space Elevator: 2nd Annual International Conference, Santa Fe, New Mexico, September 12-15, 2003;
6. J. Allyn Smith, C. Butler, *Deployment Scenarios*, The Space Elevator: 2nd Annual International Conference, Santa Fe, New Mexico, September 12-15, 2003;
7. R. D. Rugescu, *Tethered Balute Low Cost De-orbit and Recovery Project*, Paper AIAA-RS2 2004-7000, 2nd Responsive Space Conference on Rapid Development, Launch, Deployment and Operations, April 19/22, 2004, El Segundo, California, USA;
8. Forward, R. L., "Tether Transport from LEO to the Lunar Surface", AIAA Paper 91-2322, *27th Joint Propulsion Conference*, Sacramento, CA, June 1991;
9. Hoyt, R.P., Forward, R. L., "Tether Transport from Sub-Earth-Orbit to the Moon... And Back!," *1997 International Space Development Conference*, Orlando FL, May 1997;
10. Hoyt, R.P., Uphoff, C.W., "Cislunar Tether Transport System", AIAA Paper 99-2690, *35th Joint Propulsion Conference*, June 1999;
11. *** *Guide to Planetary Satellites*, Editors of *Sky & Telescope*, 2004;
12. Rothery D. *Satellites of the Outer Planets*, Clarendon Press, Oxford. 208 pp., 1992.